



## Article

# A Texture Enhancement Method for Oceanic Internal Wave Synthetic Aperture Radar Images Based on Non-Local Mean Filtering and Texture Layer Enhancement

Zhenghua Chen <sup>1</sup>, Hongcheng Zeng <sup>1</sup>, Yamin Wang <sup>1,\*</sup>, Wei Yang <sup>1</sup>, Yanan Guan <sup>1</sup> and Wei Liu <sup>2</sup>

<sup>1</sup> School of Electronics and Information Engineering, Beihang University, Beijing 100191, China; chenzhenghua@buaa.edu.cn (Z.C.); zenghongcheng@buaa.edu.cn (H.Z.); yangweigigi@buaa.edu.cn (W.Y.); guanyanan@buaa.edu.cn (Y.G.)

<sup>2</sup> School of Electronic Engineering and Computer Science, Queen Mary University of London, London E1 4NS, UK; w.liu@qmul.ac.uk

\* Correspondence: wangyamin@buaa.edu.cn

**Abstract:** Synthetic aperture radar (SAR) is an important tool for observing the oceanic internal wave phenomenon. However, owing to the unstable imaging quality of SAR on oceanic internal waves, the texture details of internal wave images are usually unclear, which is not conducive to the subsequent applications of the images. To cope with this problem, a texture enhancement method for oceanic internal wave SAR images is proposed in this paper, which is based on non-local mean (NLM) filtering and texture layer enhancement (TLE). Since the strong speckle noise commonly present in internal wave images is simultaneously enhanced during texture enhancement, resulting in degraded image quality, NLM filtering is first performed to suppress speckle noise. Then, the denoised image is decomposed into the structure layer and the texture layer, and a texture layer enhancement method oriented to the texture characteristics of oceanic internal waves is proposed and applied. Finally, the enhanced texture layer and the structure layer are combined to reconstruct the final enhanced image. Experiments are conducted based on the Gaofen-3 real SAR data, and the results demonstrate that the proposed method performs well in suppressing speckle noise, maintaining overall image brightness, and enhancing internal wave texture details.

**Keywords:** synthetic aperture radar (SAR); oceanic internal wave; texture layer enhancement (TLE); non-local mean (NLM); texture enhancement



**Citation:** Chen, Z.; Zeng, H.; Wang, Y.; Yang, W.; Guan, Y.; Liu, W. A Texture Enhancement Method for Oceanic Internal Wave Synthetic Aperture Radar Images Based on Non-Local Mean Filtering and Texture Layer Enhancement. *Remote Sens.* **2024**, *16*, 1172. <https://doi.org/10.3390/rs16071172>

Academic Editors: Zhongyu Li, Hongyang An, Yan Wang, Shiyang Tang and Alin Achim

Received: 17 February 2024  
Revised: 23 March 2024  
Accepted: 25 March 2024  
Published: 27 March 2024



**Copyright:** © 2024 by the authors. Licensee MDPI, Basel, Switzerland. This article is an open access article distributed under the terms and conditions of the Creative Commons Attribution (CC BY) license (<https://creativecommons.org/licenses/by/4.0/>).

## 1. Introduction

Oceanic internal waves are a crucial environmental factor in the marine realm, widely distributed across the world's oceans and marginal seas. Their profound impact on human activities renders them a pivotal subject of oceanographic research [1]. Oceanic internal waves have a significant impact on marine ecological protection, marine resource development, and marine military activities [2]. Research on oceanic internal waves plays an increasingly important role in the development of human marine industry and has become a hot topic of in-depth research by scholars. Applying traditional methods to observe the oceanic internal wave phenomenon is difficult to meet the requirements of obtaining large-scale information of oceanic internal waves in a short period of time, and therefore, other more effective methods are needed.

Synthetic aperture radar (SAR) can achieve all-day and all-weather observation of the Earth, and its observation is less affected by meteorological factors. The unique observational advantages of SAR enable the acquisition of large-scale information on oceanic internal waves in a short period of time, providing timely and rich data resources for their study. Currently, SAR is the primary technical tool for detecting oceanic internal waves and plays a crucial role in advancing their study [1]. However, the imaging quality of SAR

for oceanic internal waves remains unstable, resulting in unclear texture details in SAR images. To improve the quality of internal wave images and establish a solid foundation for their subsequent applications, it is necessary to study the texture enhancement methods of oceanic internal wave SAR images.

Traditionally, SAR images are mainly processed in the spatial or frequency domain to achieve image enhancement. A typical method for the former is histogram equalization, which performs grayscale transformation directly in the spatial domain, while a representative method for the latter is wavelet transform [3]. The histogram equalization method is simple and easy to implement, with outstanding real-time performance, but the enhanced image often has uneven brightness, and it may also cause the loss of texture details [4]. Oceanic internal waves typically occupy a small area in SAR images, while calm sea surfaces dominate the images, resulting in a dark overall brightness. Therefore, using histogram equalization to enhance the textures will result in over-enhancement [5]. Wavelet transform is capable of decomposing images into various frequency components. By enhancing the high-frequency components obtained from the decomposition, texture detail enhancement can be achieved [6]. Carlson employed the method to improve the contrast of oceanic SAR images, achieving significant enhancement of wave textures [7]. However, other important oceanic features in SAR images were disrupted, demonstrating the limitations of the method. Overall, these traditional methods lack pertinence to the characteristics of internal wave images, which leads to unsatisfactory results.

However, there are not many research results reported on texture enhancement for oceanic internal wave SAR images. It was found in [8] that in the process of decomposing full-polarimetric spaceborne SAR data into non-polarimetric and Bragg scattering components, oceanic phenomena such as internal waves cause more significant changes in non-polarimetric components than the cross-polarimetric ones in VV and HH polarization data. Until now, research on the enhancement of oceanic internal wave SAR images using non-polarimetric components has been mostly limited to theoretical analysis, and the exploration of its application is still relatively limited. Bai et al. [9] applied curvelet transform to decompose oceanic SAR images and enhanced specific curvelet coefficients. Although the wave texture features in the reconstructed images can be significantly enhanced, this method is prone to introducing additional noise in the enhanced images.

Our research team previously proposed a texture enhancement method based on the non-local mean (NLM) filtering and the multi-scale Retinex (MSR) algorithm to improve the contrast of oceanic internal wave SAR images [10]. The application of the NLM filtering can suppress strong speckle noise in oceanic SAR images, thus preventing speckle noise from being treated as small textures and thus enhanced, while the MSR algorithm was performed to remove low-frequency components of denoised images, thereby achieving texture detail enhancement. This method can significantly enhance the internal wave textures, but the MSR algorithm faces difficulty in achieving a satisfactory balance between high contrast and real brightness. In order to overcome the limitations of the MSR algorithm in the enhancement of oceanic internal wave SAR images, a texture enhancement method for internal waves based on the NLM filtering and the texture layer enhancement (TLE) algorithm is proposed in this work, which follows the processing order of first denoising and then texture enhancement, as adopted in [10]. Compared to [10], this paper presents the following differences or innovations:

- (1) The proposed method still employs the NLM filtering for speckle noise suppression. However, this paper effectively verifies the excellent performance of the NLM filtering in denoising and preserving texture features through richer comparative experiments. This fully demonstrates the suitability of using the NLM filtering for denoising internal wave SAR images.
- (2) The TLE algorithm is proposed in this paper to enhance the textures of internal waves. The TLE algorithm has stronger specificity for the texture features of oceanic internal waves in SAR images compared to the MSR algorithm. As a result, it has a more significant enhancement effect on internal wave textures.

- (3) The MSR algorithm alters the zero-frequency component of the image, which in turn affects the overall brightness of the image and distorts image information to some extent. In contrast, the TLE algorithm has minimal impact on the overall brightness of the image, preserving its real brightness and effectively addressing the main shortcomings of the MSR algorithm.

This paper is organized as follows. The characteristics of oceanic internal wave SAR images and details of the proposed method are presented in Section 2. In Section 3, experiments based on Gaofen-3 real SAR data are carried out to demonstrate the performance of the proposed method. In Section 4, the effect of the order of the NLM filtering and the TLE algorithm on the improvement of internal wave image quality is discussed, and conclusions are drawn in Section 5.

## 2. Materials and Methods

### 2.1. Characteristics of Oceanic Internal Wave SAR Images

#### 2.1.1. Formation Mechanism of Oceanic Internal Waves

Oceanic internal waves refer to the waves that propagate within the ocean. If seawater at different depths is stably stratified due to different densities, and there is a disturbance source that disrupts this stable stratification phenomenon, it is possible to form oceanic internal waves at the interface of seawater with different densities. The stable stratification of fluids and the presence of disturbance sources are necessary conditions for the generation of oceanic internal waves. If the heat emitted by the sun is continuously absorbed by seawater, the temperature of seawater near the sea surface will be significantly higher than that of deeper seawater. The higher temperature reduces the density of the near-surface layer of the ocean, leading to the formation of a more stable layered structure in seawater. If there is a disturbance source that disturbs the area with the highest density change in seawater, it will lead to the generation of oceanic internal waves [1].

Figure 1 provides a schematic diagram of the phenomenon of oceanic internal waves, where the waves at the junction of the low-density layer and the high-density layer are referred to as oceanic internal waves. A transparent plastic toy box containing two layers of liquids of different colors, which are of different densities and cannot be fused, can be used to describe the generation of internal waves in a simple and vivid way. These two liquids fill the entire box. When the box tilts or shakes, a large amplitude, low-speed wave propagates along the interface between the two layers of liquids, which is called an internal wave.

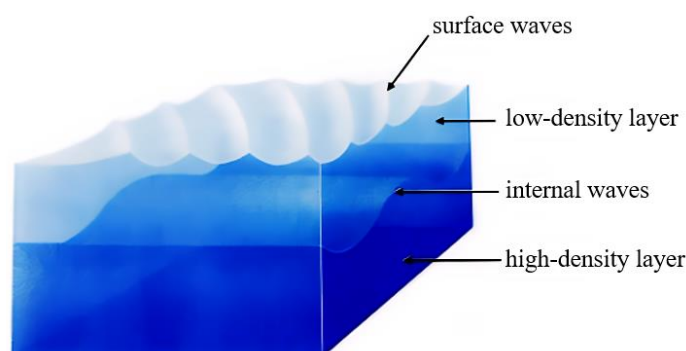


**Figure 1.** Schematic diagram of the phenomenon of oceanic internal waves.

As one of the necessary conditions for the generation of internal waves, the stable stratification of seawater is often satisfied because the density of seawater is usually unevenly distributed, and there are many factors that may serve as the disturbance sources, including sailing ships, seabed earthquakes, interaction between undulating seabed topography and strong oceanic currents or gravitational tides. As a result, the generation of internal waves is frequent, making them a common oceanic phenomenon.

### 2.1.2. Characteristics of Oceanic Internal Wave SAR Images

In order to effectively improve the image quality, it is necessary to understand the main characteristics of oceanic internal wave SAR images.

The wavelength of SAR is situated in the microwave band, which limits its ability to penetrate seawater. As a result, SAR cannot directly detect oceanic internal waves, which propagate within the ocean [11]. However, according to the imaging mechanism of SAR, SAR can indirectly detect oceanic internal waves. The schematic diagram illustrating the formation of the SAR signature of oceanic internal waves is presented in Figure 2. The existence of the pycnocline in seawater is a necessary condition for the generation of internal waves. Line (a) in Figure 2 shows the shape of the pycnocline when internal waves propagate forward. The vertical displacement of the pycnocline results in a roughness pattern shown by line (b) in Figure 2 on the sea surface. The pattern contains pairs of adjacent rough and smooth strips, which are separated by broad areas with average roughness. Oceanic internal waves become visible in SAR images due to the variation in the sea surface roughness [12,13], and the specific mechanism can be explained by [14]

$$\sigma = \sigma_0 \left( 1 + A \frac{dU_x}{dx} \right) \quad (1)$$

where  $\sigma$  is the total normalized radar cross section (NRCS),  $\sigma_0$  is the NRCS of the background,  $x$  is the coordinate in the direction of the look direction of the SAR antenna projected onto the horizontal plane,  $dU_x/dx$  is the surface current gradient, and  $A$  is a constant that depends on wavelength, incidence angle, and relaxation rate [14]. In (1), the gradient  $dU_x/dx$  is increased in rough regions and is decreased in smooth regions, which causes the radar signature of internal waves to manifest itself in SAR images as strips of increased and decreased NRCS relative to the background. Consequently, as line (c) in Figure 2 shows, oceanic internal waves are characterized by pairs of adjacent bright and dark stripes in a uniform background in SAR images [15,16].

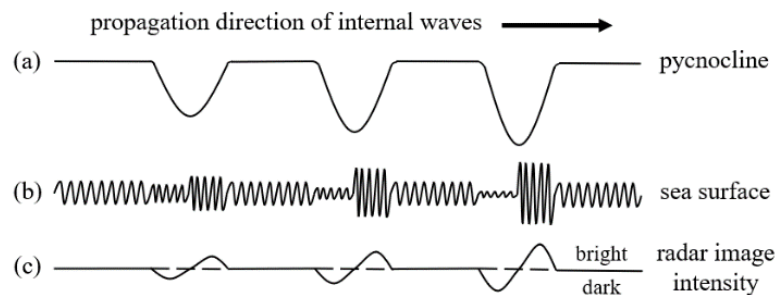


**Figure 2.** Schematic diagram illustrating formation of SAR signature of oceanic internal waves: (a) shape of pycnocline; (b) roughness pattern on sea surface; (c) variation in radar image intensity (image brightness).

In addition, it can be noted that the width of the bright and dark stripes in Figure 2 is much smaller than the width of the region with average image brightness. Therefore, most areas of an internal wave SAR image are the background with average grayscale, and the bright and dark stripes of internal waves in the uniform background are relatively narrow [14]. In other words, the large-scale structure of an internal wave SAR image is relatively flat, and the textures of internal waves are characterized by long and thin stripes with directionality.

The influence of speckle noise should be considered when enhancing the textures. Texture enhancement is the process of increasing the degree of grayscale variation [10]. When enhancing the textures of oceanic internal wave SAR images, the strong speckle noise caused by unstable imaging quality is easily mistaken for small textures and is thus enhanced, which is not conducive to improving image quality. Hence, speckle noise suppression is an indispensable step when performing texture enhancement on these images.

## 2.2. Data Introduction

This paper presents the results of texture enhancement experiments conducted on five real oceanic internal wave SAR images obtained by the Gaofen-3 satellite over the South China Sea region. The satellite is China's first C-band multipolar SAR imaging satellite with a 1 m resolution, and can provide stable and reliable SAR images with technical features such as high resolution, wide swath, multiple imaging modes, and long lifespan operation. The selected SAR images are all located near the Dongsha Islands, where oceanic internal waves are frequent. Figure 3 shows the approximate position of the selected internal wave SAR images, indicated by the red dotted box centered on the Dongsha Islands. Furthermore, Table 1 provides detailed information on the five SAR images of oceanic internal waves mentioned above. For all oceanic internal wave SAR images presented in this paper, it should be noted that the vertical direction of SAR images is the azimuth direction, and the horizontal direction is the range direction.



**Figure 3.** Approximate position of the selected internal wave SAR images. (The red dotted box centered on the Dongsha Islands reflects the approximate position of the real oceanic internal wave scenes corresponding to the selected SAR images).

**Table 1.** Detailed information of the selected five oceanic internal wave SAR images.

Number	Scene Center Position	Data Acquisition Date [UTC]	Imaging Mode	Polarization
Data1	(116.2°E, 20.9°N)	26 July 2019	UFS <sup>1</sup>	HH
Data2	(114.9°E, 21.2°N)	3 March 2018	UFS	HH
Data3	(115.0°E, 20.9°N)	3 March 2018	UFS	HH
Data4	(116.3°E, 21.4°N)	20 July 2021	UFS	HH
Data5	(115.1°E, 20.7°N)	5 September 2018	UFS	HH

<sup>1</sup> UFS: Ultrafine stripe mode.

## 2.3. Texture Enhancement Method

To ensure high image quality, it is crucial to suppress speckle noise before enhancing the textures of oceanic internal waves, because the texture enhancement operation will amplify the speckle noise, leading to a significant reduction in image quality. For texture enhancement of denoised images, the main characteristics of oceanic internal wave SAR images should be taken into consideration. Based on the above considerations, as shown in Figure 4, the proposed method includes two steps: the NLM filtering for image denoising and the TLE algorithm for texture enhancement.

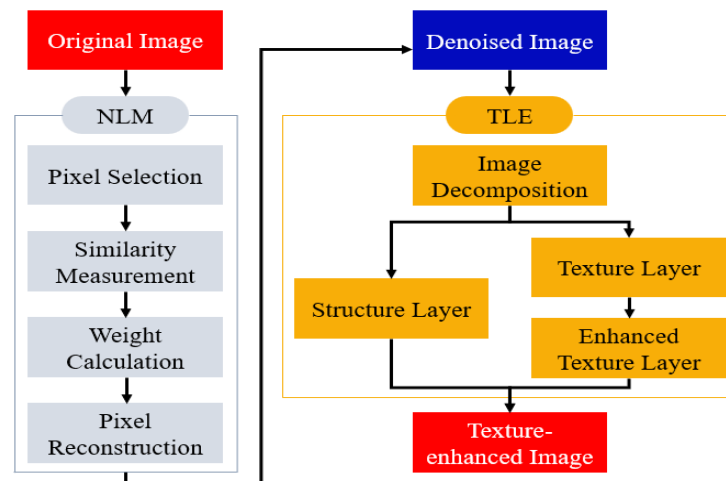


**Figure 4.** Illustration of the proposed method.

### 2.3.1. Non-Local Mean Filtering

The first step is the NLM filtering to prevent speckle noise from interfering with the texture enhancement process. Details of the NLM filtering process are presented as follows.

Given a discrete noisy image  $v = \{v(i) | i \in I\}$ , for a pixel  $i$ , its grayscale value in the denoised image can be obtained by calculating the weighted average of the grayscale values of all pixels in the search area, using [17]

$$\hat{v}(i) = \sum_{j \in S} w(i, j) v(j) \quad (2)$$

where  $\{w(i, j)\}_j$  are the normalized weights satisfying  $0 \leq w(i, j) \leq 1$  and  $\sum_{j \in S} w(i, j) = 1$ , and  $S$  is the pre-set search area, typically a large window centered at the target pixel  $i$ .

The similarity between two pixels  $i$  and  $j$  depends on the weighted Euclidean distance between their respective square window neighborhoods  $v(N_i)$  and  $v(N_j)$ . The weighted Euclidean distance can be calculated by [17]

$$d(i, j) = \|v(N_i) - v(N_j)\|_{2,a}^2 \quad (3)$$

where  $a > 0$  is the standard deviation of the Gaussian kernel.

When calculating the grayscale value of the target pixel  $i$  in the denoised image, the corresponding weight of the pixel  $j$  is defined as [17]

$$w(i, j) = e^{-\frac{d(i, j)}{h^2}} / Z(i) \quad (4)$$

where  $Z(i) = \sum_j e^{-\frac{d(i, j)}{h^2}}$  is the normalization constant, and  $h$  is the parameter that controls the degree of noise suppression.

### 2.3.2. Texture Layer Enhancement

#### 1. Separation of Structure Layer and Texture Layer

An image can be decomposed into a structure layer and a texture layer. The structure layer contains large-scale structural information of the image, while the texture layer contains its texture details. Effective separation of the two layers is the premise of texture layer enhancement. To separate them, Xu et al. [18] proposed a structure layer extraction method based on relative total variation. The method contains a general pixel-wise windowed total variation measure, given by [18]

$$D_x(p) = \sum_{q \in R(p)} g_{p,q} \cdot |(\partial_x S)_q| \quad (5)$$

where the pixel  $q$  belongs to  $R(p)$ , the rectangular region centered at the pixel  $p$ ,  $S$  is the structure layer, and  $g_{p,q}$  is a weighting function, expressed as [18]

$$g_{p,q} \propto \exp\left(-\frac{(x_p - x_q)^2 + (y_p - y_q)^2}{2\sigma^2}\right) \quad (6)$$

where  $\sigma$  controls the spatial scale of the window,  $x_p$  and  $y_p$  are the coordinates of  $p$  in the  $x$  and  $y$  directions, respectively. Similarly,  $x_q$  and  $y_q$  are the coordinates of  $q$  in the  $x$  and  $y$  directions, respectively.

Besides  $D$ , the method also contains a novel windowed inherent variation, expressed as [18]

$$L_x(p) = \left| \sum_{q \in R(p)} g_{p,q} \cdot (\partial_x S)_q \right| \quad (7)$$

As for  $D_y(p)$  and  $L_y(p)$ , they are consistent with the form in the  $x$  direction.

The method combines  $D$  with  $L$  to form a regularizer for structure-texture decomposition. The objective function is expressed as [18]

$$\operatorname{argmin}_S \sum_p (S_p - I_p)^2 + \lambda \cdot \left( \frac{D_x(p)}{L_x(p) + \varepsilon} + \frac{D_y(p)}{L_y(p) + \varepsilon} \right) \quad (8)$$

where  $I$  is the original image,  $\lambda$  is a weight, and  $\varepsilon$  is a small positive number to avoid division by zero. The structure layer of the original image can be obtained by minimizing the objective function shown in (8).

## 2. Texture Layer Enhancement

Texture layer enhancement is the core of the proposed method. In order to facilitate texture layer enhancement, we express the relationship between the original image, the structure layer and the texture layer as follows:

$$I(i, j) = S(i, j) \times T(i, j) \quad (9)$$

where  $(i, j)$  is the two-dimensional spatial coordinates of the pixel, and  $T$  is the texture layer. Both  $I(i, j)$  and  $S(i, j)$  in (9) have been normalized, i.e., the following conditions are satisfied:  $0 \leq I(i, j) \leq 1$  and  $0 \leq S(i, j) \leq 1$ .

After the structure layer is acquired, the texture layer can be obtained through (9). As shown in (9), the original image is the product of the structure layer and the texture layer. Hence, similar to that in digital communication, the amplitude of the sinusoidal carrier signal is modulated by the digital baseband signal, the original image can be considered as the result of the structure layer being modulated by the texture layer.

Since  $I(i, j)$  and  $S(i, j)$  in (9) have been normalized, if  $I(i, j) > S(i, j)$ ,  $T(i, j)$  will be larger than one, and if  $I(i, j) < S(i, j)$ ,  $T(i, j)$  will be smaller than one. The uniform background and texture characteristics of internal wave SAR images make the  $T(i, j)$  corresponding to bright stripes larger than one, and the  $T(i, j)$  corresponding to dark stripes smaller than one. Based on this, the texture layer can be enhanced by

$$T^*(i, j) = [T(i, j)]^\alpha \quad (10)$$

where  $T^*$  is the enhanced texture layer, and  $\alpha$  is the texture enhancement parameter.  $\alpha$  should be larger than one. The larger  $\alpha$  is, the stronger the modulation effect, and thus the greater the difference between bright and dark stripes of internal waves.

Finally, the structure layer and the enhanced texture layer are combined to reconstruct the final enhanced image  $I^*$ :

$$I^*(i, j) = S(i, j) \times T^*(i, j) \quad (11)$$

## 2.4. Image Quality Evaluation

This paper adopts objective evaluation indexes to accurately evaluate the performance of relevant algorithms. When evaluating denoising algorithms, the equivalent number of looks  $ENL$  is adopted to measure the speckle noise intensity of SAR images and determine the noise suppression effect. The larger  $ENL$  is, the lower the intensity of speckle noise in SAR images. In addition, the structural similarity  $SSIM$  is adopted to measure the similarity of texture details before and after denoising in SAR images to determine the effectiveness of denoising algorithms in preserving image texture details. A larger  $SSIM$  indicates that the texture details of the image are preserved better after denoising.

Currently, most SAR image quality evaluation indexes are aimed at land images, especially for land point targets, while there are very few objective evaluation indexes for oceanic internal wave SAR images. To address this issue, Ref. [19] proposed a set of objective evaluation indexes mainly for the texture characteristics of oceanic internal waves. This paper evaluates the texture enhancement effect using two indexes proposed in [19]: the margin between positive and negative modulation  $S_{BD}$  and the weighing relative NRCS  $\Delta\sigma_w^0$ . A larger  $S_{BD}$  represents more intensity difference between bright and dark stripes of internal waves, while a larger  $\Delta\sigma_w^0$  indicates greater clarity of internal wave textures. In addition, this paper also evaluates the texture enhancement effect using three other indexes: mean  $m$ , variance  $Var$ , and contrast  $C$ .

## 3. Results

### 3.1. Texture Layer Enhancement Experiments

To verify the significant texture enhancement effect of the proposed TLE algorithm on oceanic internal wave SAR images, Data1 is first used for texture enhancement experiments. The original image of Data1 and the results of each step obtained during its processing by the TLE algorithm are presented in Figure 5. As presented in Figure 5a, the clarity of internal wave texture details in this unprocessed SAR image is low and requires improvement. Additionally, the original image is accompanied by obvious speckle noise. When the TLE algorithm is directly applied to Figure 5a, the structure layer and texture layer obtained from image decomposition are presented in Figure 5b,c respectively. The TLE algorithm's ability to effectively separate the two layers has a direct impact on the final texture enhancement result. Figure 5b,c demonstrate the proposed TLE algorithm's success in this regard, providing a solid foundation for the subsequent texture layer enhancement operation. In the structure layer, the texture details are smoothed out, leaving only the large-scale image structural information. In the texture layer, numerous gully-like textures can be found, and the texture details in the original image are all contained in the texture layer. Additionally, speckle noise is also extracted into the texture layer because it can cause fluctuations in grayscale. Figure 5d displays the enhanced texture layer. As demonstrated, the shadows in the texture layer are deepened, the stripe undulations become more severe, and the gully-like textures are significantly enhanced. However, the speckle noise is also amplified to a severe degree. Ultimately, the enhanced texture layer is combined with the structure layer to reconstruct the final enhanced image shown in Figure 5e. Comparing Figure 5a,e, it is evident that the TLE algorithm enhances the texture details of oceanic internal waves markedly, while the intensity of speckle noise increases significantly, leading to a decrease in image quality. The experimental results suggest that to prevent speckle noise from interfering with the texture enhancement process, it is necessary to suppress speckle noise before applying the TLE algorithm for texture enhancement.

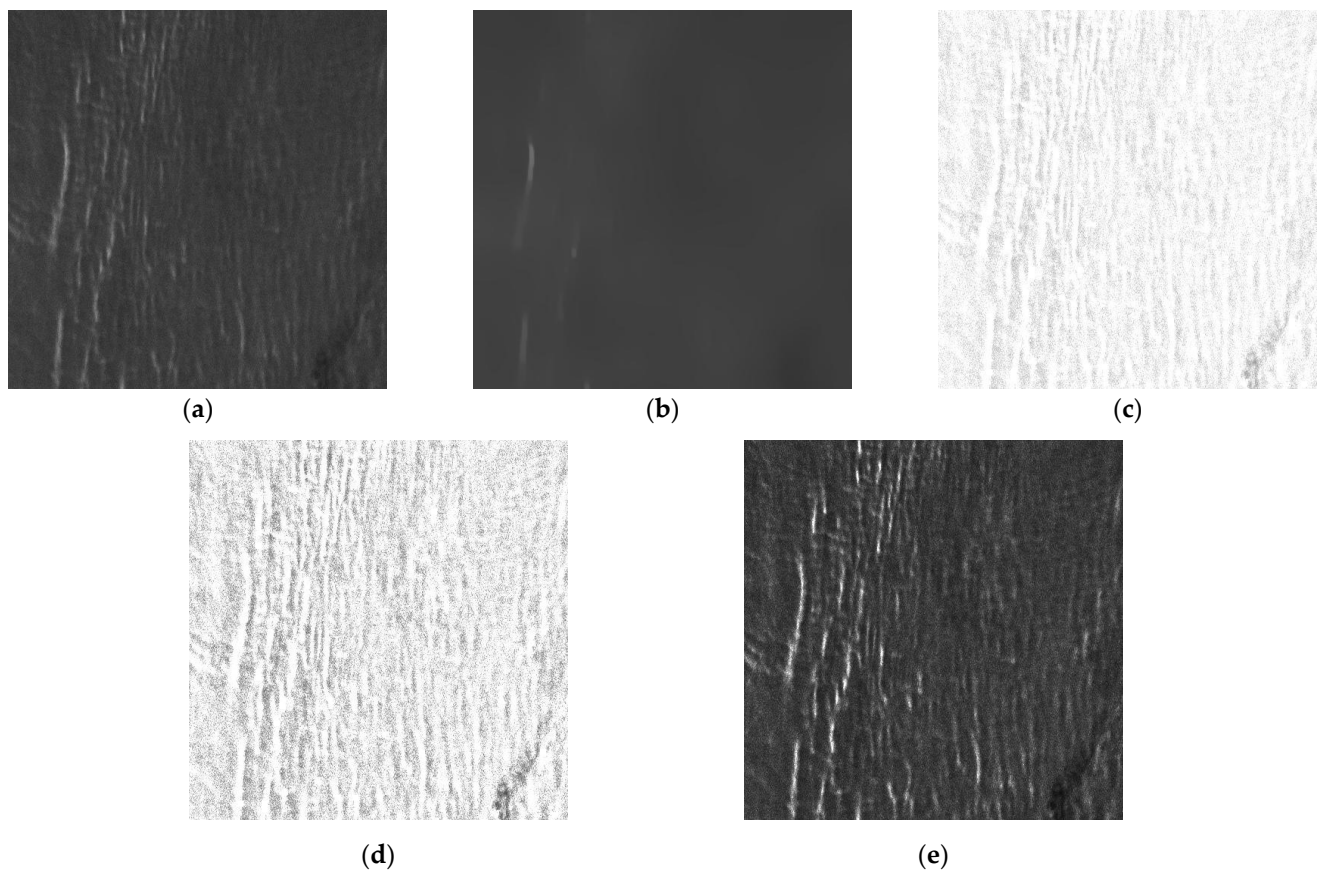


**Figure 5.** Results of each step in the processing of Data1 by TLE algorithm: (a) original image; (b) structure layer; (c) texture layer; (d) enhanced texture layer; (e) texture enhancement result by TLE algorithm.

The objective indexes of Data1 and its final texture enhancement result by the TLE algorithm are listed in Table 2. As can be seen, applying the TLE algorithm directly to the original SAR image for texture enhancement results in a noteworthy improvement in texture indexes and a significant reduction in the *ENL*. This indicates that the TLE algorithm enhances the texture details of oceanic internal waves and speckle noise without differentiation, which is consistent with the conclusion drawn by visual observation of experimental results, again demonstrating the necessity of performing the denoising operation before texture enhancement.

**Table 2.** Objective indexes of Data1 and its final texture enhancement result by TLE algorithm.

	<i>ENL</i>	<i>m</i>	<i>Var</i>	<i>C</i>	<i>S<sub>BD</sub></i> (dB)	$\Delta\sigma_w^0$ (dB)
Original	35.67	58.45	109.92	0.35	1.00	0.54
TLE	5.35	58.38	1009.66	1.35	2.40	3.42

### 3.2. Comparison of Different Denoising Methods

The texture enhancement experiments based on the TLE algorithm suggest that denoising is an indispensable step before adopting this algorithm to enhance the textures of oceanic internal wave SAR images. Therefore, the proposed method first suppresses speckle noise in SAR images by performing the NLM filtering before texture layer enhancement. To assess the effectiveness of the NLM filtering in preserving image texture details while denoising, it is essential to conduct experiments comparing its performance with other SAR image denoising methods.

This section presents the results of experiments conducted on three typical SAR image denoising methods: the Lee filter [20], the SAR-oriented version of block-matching 3-D (SAR-BM3D) algorithm [21], and the NLM filtering. Among them, the Lee filter is a classic method that utilizes the local statistical characteristics of images for speckle noise suppression, and the SAR-BM3D algorithm is a SAR image denoising method that combines non-local filtering and wavelet-domain shrinkage. The SAR-BM3D algorithm is an improvement of the BM3D algorithm [22], which is suitable for additive white Gaussian noise denoising, and is adapted to the characteristics of SAR image speckle noise. The experiments are based on the five real oceanic internal wave SAR images introduced in the previous section, in order to evaluate the comprehensive performance of the three methods in denoising and preserving image texture details.

The processing results are presented in Figure 6. As shown, all five internal wave images are accompanied by a certain level of speckle noise. Visual observation reveals that the Lee filter has a limited suppression effect on speckle noise, and there is still significant noise remaining in the denoised images. At the same time, the texture details of the images are largely smoothed, making the denoised images more blurred and reducing the image resolution. The SAR-BM3D algorithm and the NLM filtering effectively suppress speckle noise and there is no obvious residual noise in the denoised images. Additionally, both methods have preserved the image texture details well, but the NLM filtering has a slightly better result.

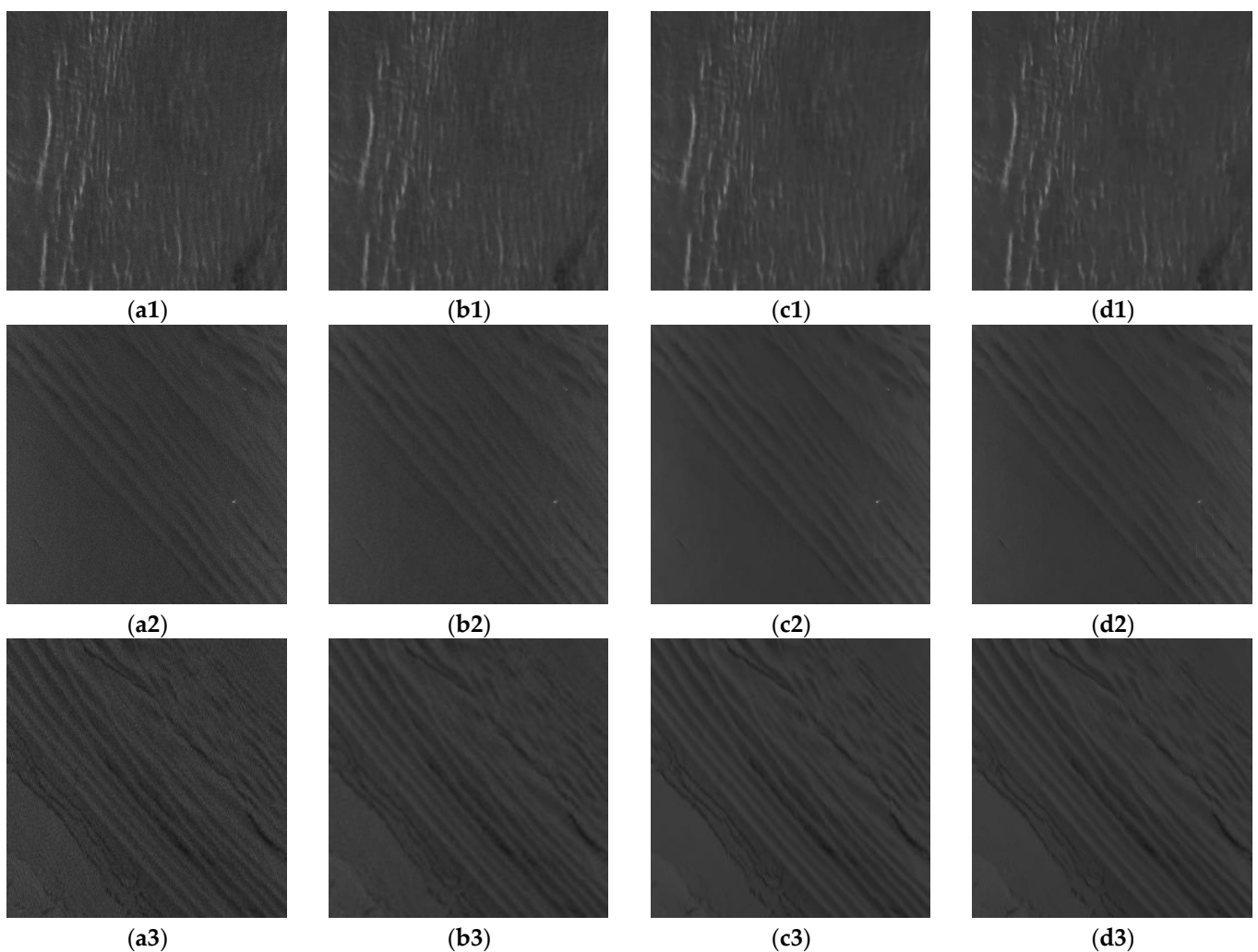
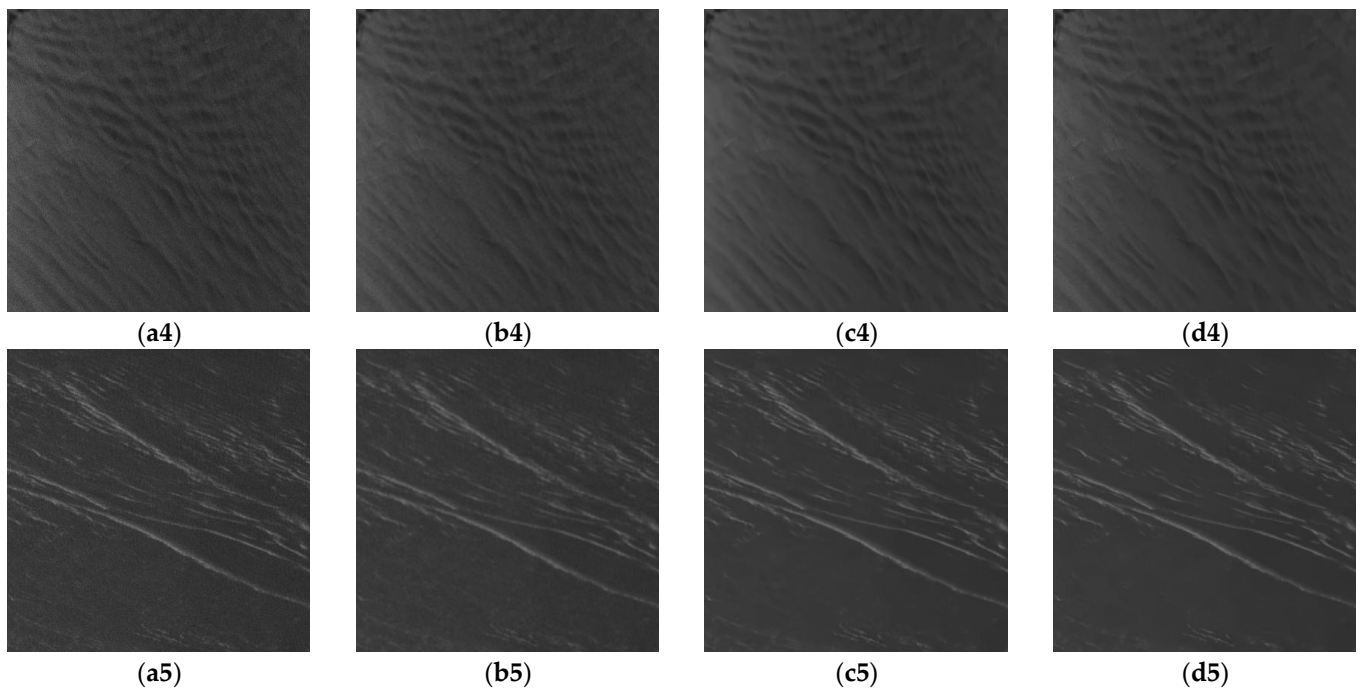


Figure 6. Cont.



**Figure 6.** Processing results of three denoising methods on five internal wave images: (a1–a5) are the original images of Data1–Data5, respectively; (b1–b5) are the processing results of the Lee filter for Data1–Data5, respectively; (c1–c5) are the processing results of the SAR-BM3D algorithm for Data1–Data5, respectively; (d1–d5) are the processing results of the NLM filtering for Data1–Data5, respectively.

In order to demonstrate their performance in a more intuitive way, grayscale profiles are taken at the same positions in the images before and after denoising, as shown in Figure 7. In the profile, the red line reflects the grayscale fluctuations of the original image along the red arrow. Large line fluctuations generally correspond to the stripes of oceanic internal waves, while small ones are generally caused by speckle noise. As shown in Figure 7, all three denoising methods can reduce the fluctuation of the red lines corresponding to the original images, which indicates that the three denoising methods can not only suppress the image speckle noise, but also smooth the internal wave texture details to some extent. It is easy to find that the NLM filtering and the SAR-BM3D algorithm have a significantly better suppression effect on speckle noise than the Lee filter. At the same time, the locally enlarged images of internal wave stripes in grayscale profiles demonstrate that the Lee filter has the strongest smoothing effect on internal wave stripes, resulting in an unsatisfactory texture detail preservation effect. And the NLM filtering has an overall better preservation effect on internal wave stripes than the SAR-BM3D algorithm, causing only slight changes in the grayscale of stripes, which provides a good basis for the subsequent texture enhancement step.

Next, the objective indexes introduced in the previous section are calculated and listed in Table 3. As can be seen, the Lee filter has the smallest improvement in the *ENL*, and the *SSIM* of the denoised images by the Lee filter is the smallest, which indicates that the performance of the Lee filter is the worst in terms of noise suppression and texture feature preservation. However, both the SAR-BM3D algorithm and the NLM filtering significantly improve the *ENL* of internal wave images, and the *SSIM* of the denoised images by the two methods is relatively large. It suggests that the overall performance of the SAR-BM3D algorithm and the NLM filtering in denoising and texture feature preservation is relatively satisfactory. It is important to note that the denoised images' *ENL* is larger by the SAR-BM3D algorithm than that by the NLM filtering, while the *SSIM* is usually smaller than that of the NLM filtering. This indicates that the SAR-BM3D algorithm exhibits a powerful

denoising effect on internal wave images, albeit at the cost of sacrificing texture details to some extent. Therefore, compared with the SAR-BM3D algorithm, the NLM filtering achieves a better balance between denoising and texture feature preservation.

As listed in Table 3, since all three denoising methods have a certain smoothing effect on the texture features of internal wave images, the texture indexes of the images decrease after denoising. Of the three methods, the Lee filter typically results in the greatest reduction in texture indexes of the denoised images due to its poor texture feature preservation performance, while the SAR-BM3D algorithm and the NLM filtering result in similar reductions. It is worth noting that all three methods have little effect on the mean values of the internal wave images. In conclusion, among the three, the SAR-BM3D algorithm and NLM filtering have a better overall performance. However, in comparison to the SAR-BM3D algorithm, the NLM filtering achieves a better balance between denoising and texture feature preservation. Considering the SAR-BM3D algorithm's high computational load and low efficiency, and the moderate and more acceptable complexity of the NLM filtering, it is more preferable to adopt the NLM filtering for denoising oceanic internal wave SAR images prior to texture enhancement.

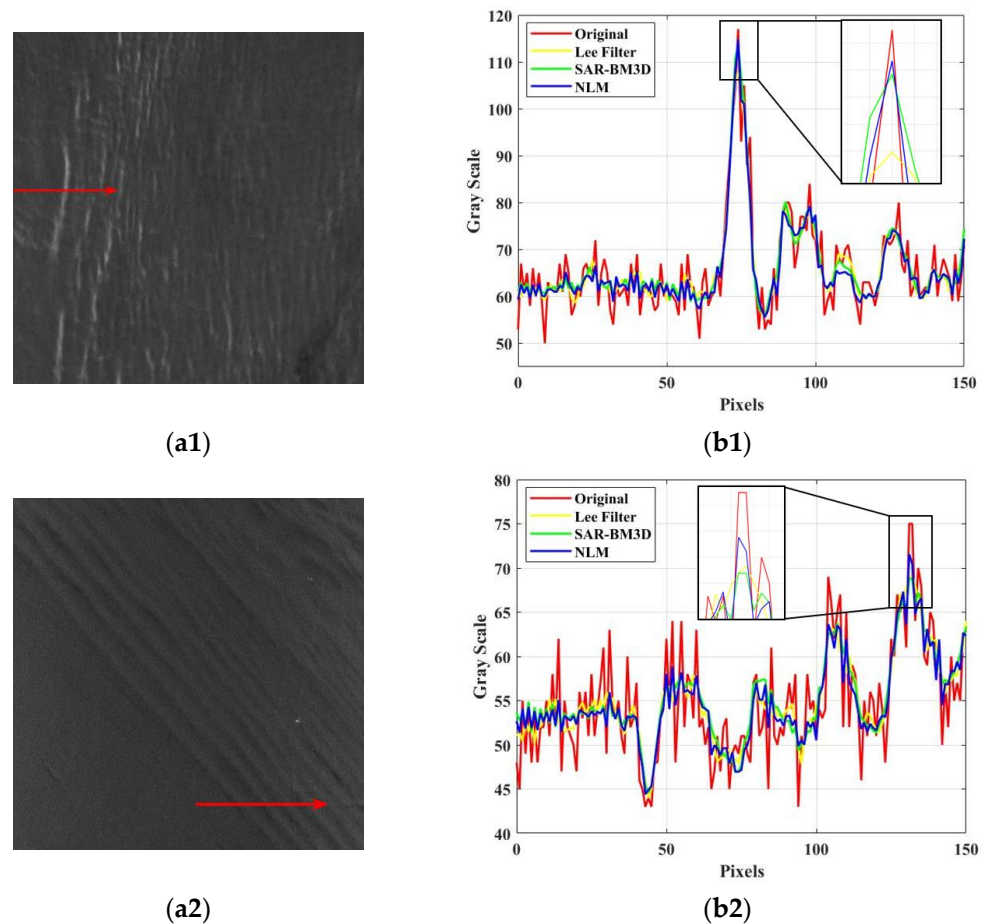
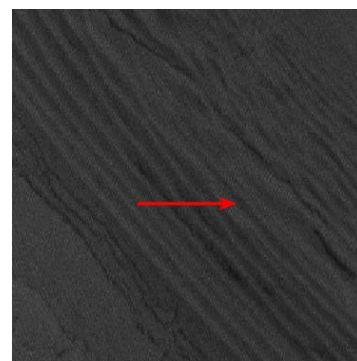
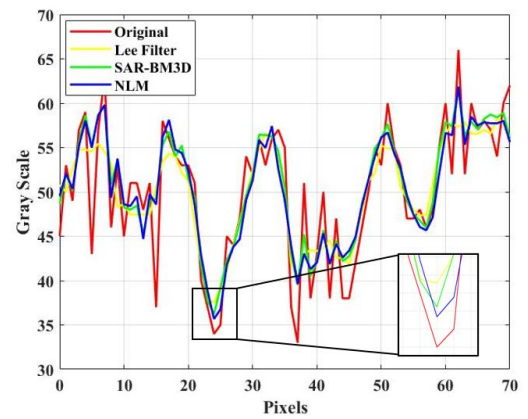


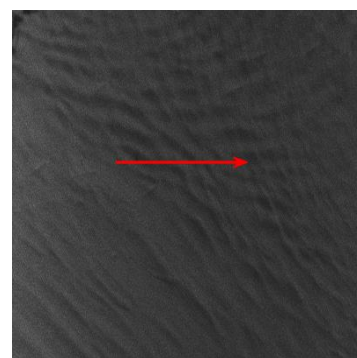
Figure 7. Cont.



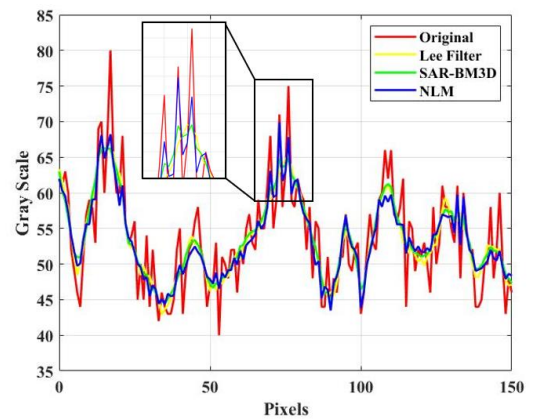
(a3)



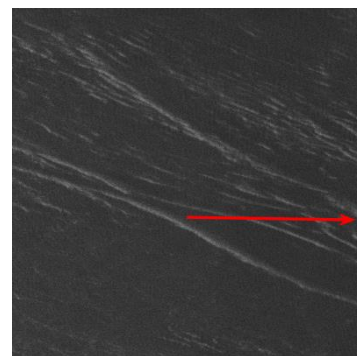
(b3)



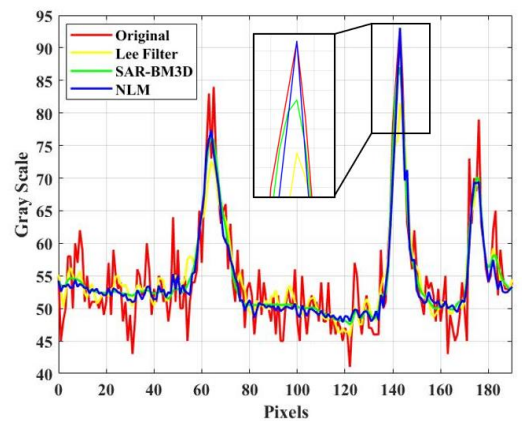
(a4)



(b4)



(a5)



(b5)

**Figure 7.** Grayscale profiles of denoised images: The red arrows in (a1–a5) respectively display the positions of grayscale profiles of Data1–Data5; (b1–b5) are grayscale profiles of the original images and the denoised images by the three denoising methods of Data1–Data5, respectively.

**Table 3.** Objective indexes of denoising experiment results.

		<i>ENL</i>	<i>SSIM</i>	<i>m</i>	<i>Var</i>	<i>C</i>	<i>S<sub>BD</sub></i> (dB)	$\Delta\sigma_w^0$ (dB)
Data1	Original	35.67	/	58.45	109.92	0.35	1.00	0.54
	Lee Filter	127.58	0.56	58.45	73.31	0.29	0.82	0.37
	SAR-BM3D	205.28	0.62	58.61	84.68	0.31	0.85	0.41
	NLM	277.17	0.73	58.44	87.91	0.32	0.86	0.41

Table 3. Cont.

		ENL	SSIM	$m$	Var	C	$S_{BD}$ (dB)	$\Delta\sigma_w^0$ (dB)
Data2	Original	41.60	/	54.37	36.25	0.23	0.79	0.14
	Lee Filter	266.52	0.31	54.39	18.20	0.16	0.60	0.07
	SAR-BM3D	1408.56	0.44	54.60	17.55	0.16	0.59	0.07
	NLM	829.10	0.60	54.43	18.30	0.16	0.59	0.07
Data3	Original	29.11	/	60.03	58.12	0.30	1.10	0.24
	Lee Filter	226.20	0.53	60.00	32.42	0.22	0.85	0.13
	SAR-BM3D	320.21	0.74	60.02	38.08	0.24	0.91	0.16
	NLM	288.23	0.72	59.91	35.77	0.24	0.88	0.15
Data4	Original	42.21	/	60.65	44.51	0.25	0.89	0.18
	Lee Filter	227.03	0.42	60.60	26.17	0.19	0.71	0.11
	SAR-BM3D	489.91	0.47	60.63	25.71	0.19	0.71	0.11
	NLM	399.06	0.61	60.39	25.84	0.19	0.71	0.11
Data5	Original	31.82	/	55.47	99.97	0.37	1.09	0.38
	Lee Filter	211.83	0.60	55.48	56.23	0.27	0.83	0.22
	SAR-BM3D	1789.24	0.70	55.45	74.16	0.32	0.93	0.28
	NLM	1257.28	0.70	55.01	68.64	0.31	0.92	0.25

### 3.3. Experimental Results of Texture Enhancement by the Proposed Method

The experimental results in the previous sections have separately verified the effectiveness of the two steps included in the proposed method, i.e., the NLM filtering and the TLE algorithm. This section combines the two steps and presents experimental results to validate the overall effectiveness of the proposed method. Moreover, the method in [10] is included for comparison. The texture enhancement results by both methods are presented in Figure 8. It can be seen that both methods significantly suppress speckle noise in internal wave images, thus avoiding the negative effects of noise on texture enhancement; they also enhance internal wave texture details, but the proposed method has a more pronounced effect. Furthermore, it is evident that the method in [10] considerably alters the overall brightness of the internal wave images, leading to distortion of the image information to a certain extent, while the proposed method has little effect on the overall brightness of the images.

The grayscale profiles are displayed in Figure 9, where the positions of grayscale profiles are the same as in Figure 7. It can be observed that both methods amplify the grayscale fluctuations, making the internal wave stripes visually clearer. The method in [10] changes the mean values of the internal wave images to varying degrees, thereby affecting the overall brightness of the images, while the proposed method effectively maintains the mean values of the images. When the method in [10] has a small and acceptable effect on image brightness (Data1, Data2, Data5), its amplification effect on grayscale fluctuations is inferior to that of the proposed method. However, when the method in [10] has a larger amplification effect on grayscale fluctuations than the proposed one (Data3, Data4), the image brightness has been severely changed by the method in [10], resulting in distorted image information.

Similar conclusions can be drawn from the objective indexes listed in Table 4. Both methods significantly improved the ENL and texture indexes of the images, as listed in Table 4. The proposed method maintains the mean values of the images as almost unchanged, while the mean value preservation effect of the method in [10] is unsatisfactory. Moreover, the proposed method generally improves the values of  $C$ ,  $S_{BD}$ , and  $\Delta\sigma_w^0$  of the images to a better extent than the method in [10]. When the method in [10] has a small change in image mean values (Data1, Data2, Data5), its improvement in the ENL and Var is inferior to the proposed method. However, when the method in [10] has a better improvement in these two indexes (Data3, Data4), the image mean values have been changed unacceptably. In conclusion, the proposed method has excellent performance in

suppressing speckle noise, maintaining overall brightness, and enhancing texture details in oceanic internal wave SAR images.

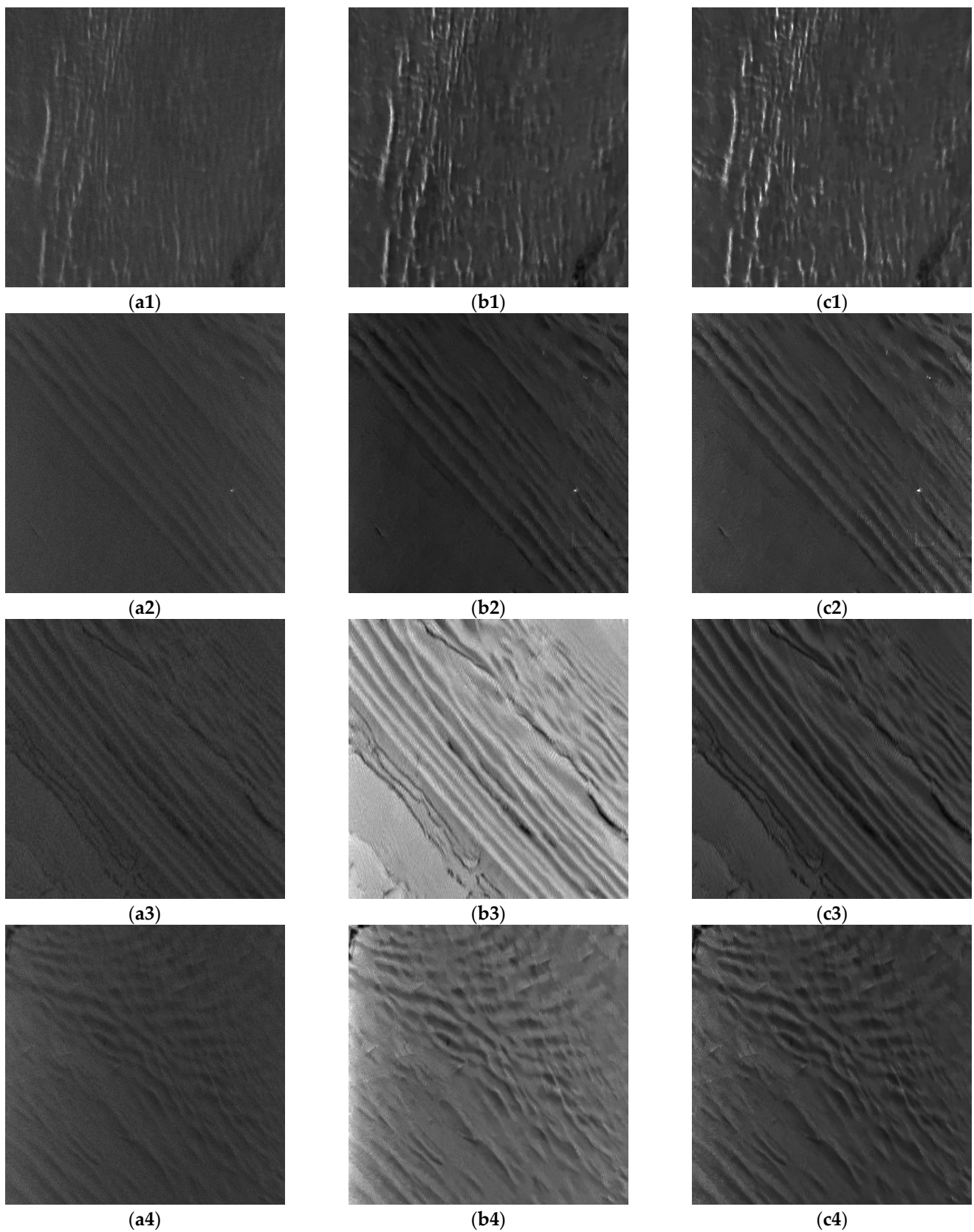
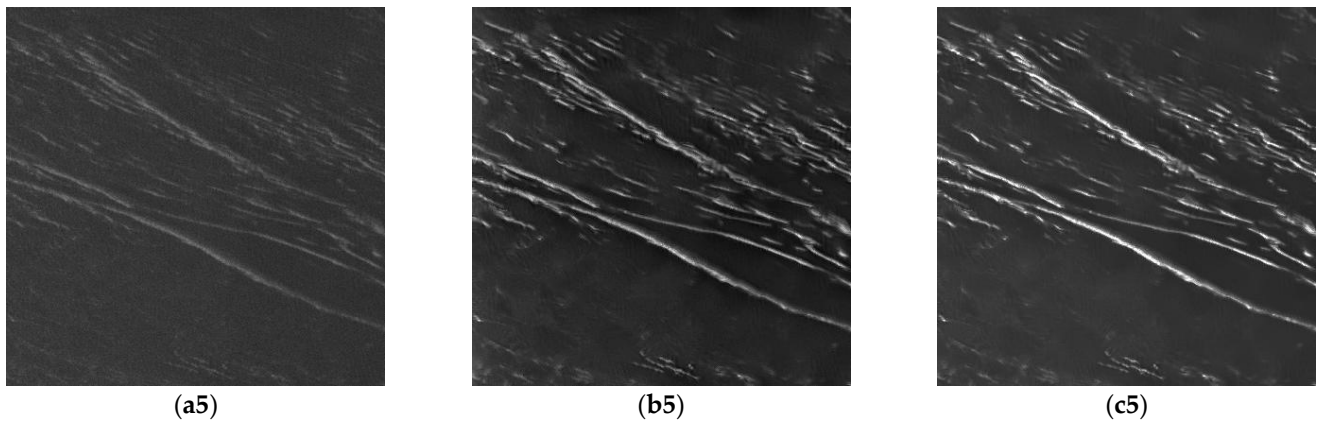
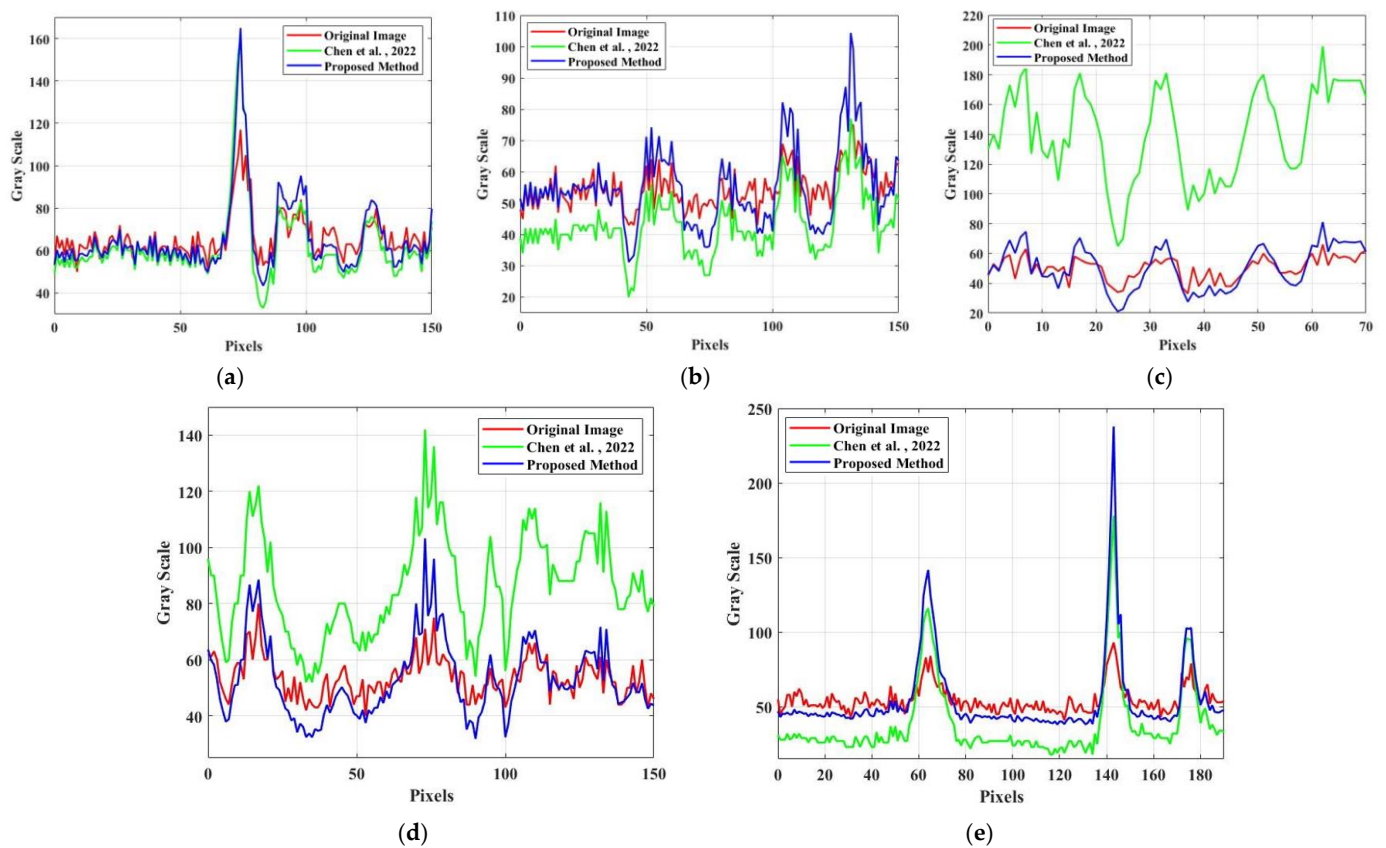


Figure 8. Cont.



**Figure 8.** Texture enhancement results of the method in [10] and the proposed method: (a1–a5) are the original images of Data1–Data5, respectively; (b1–b5) are the texture enhancement results of the method in [10] for Data1–Data5, respectively; (c1–c5) are the texture enhancement results of the proposed method for Data1–Data5, respectively.



**Figure 9.** Grayscale profiles of texture enhancement results by the method in [10] and the proposed method: (a–e) are grayscale profiles of Data1–Data5, respectively, and the “Chen et al., 2022” in the grayscale profiles represents the method in [10]. The positions of grayscale profiles are the same as in Figure 7.

**Table 4.** Objective indexes of texture enhancement results.

		<i>ENL</i>	<i>m</i>	<i>Var</i>	<i>C</i>	<i>S<sub>BD</sub></i> (dB)	$\Delta\sigma_w^0$ (dB)
Data1	Original Image	35.67	58.45	109.92	0.35	1.00	0.54
	Method in [10]	54.69	57.96	384.35	0.74	1.74	1.42
	Proposed Method	58.95	57.94	583.83	1.02	1.83	2.00
Data2	Original Image	41.60	54.37	36.25	0.23	0.79	0.14
	Method in [10]	73.19	38.57	96.98	0.48	1.73	0.37
	Proposed Method	95.54	53.79	172.87	0.52	1.76	0.60
Data3	Original Image	29.11	60.03	58.12	0.30	1.10	0.24
	Method in [10]	83.57	169.65	934.29	0.42	1.72	0.51
	Proposed Method	35.88	64.01	190.74	0.54	2.17	0.78
Data4	Original Image	42.21	60.65	44.51	0.25	0.89	0.18
	Method in [10]	112.17	94.30	295.79	0.39	1.54	2.25
	Proposed Method	79.81	62.72	154.90	0.46	1.77	0.62
Data5	Original Image	31.82	55.47	99.97	0.37	1.09	0.38
	Method in [10]	46.31	39.94	806.54	1.25	3.10	1.88
	Proposed Method	162.29	54.83	967.30	1.30	2.53	2.31

#### 4. Discussion

Because the texture enhancement step intensifies the speckle noise, the proposed method first applies the NLM filtering to denoise the image before performing the TLE algorithm to enhance texture details, which effectively reduces the negative impact of speckle noise on image quality improvement. One may ask whether the order of the NLM filtering and the TLE algorithm can be changed, and in the following, we show that the answer to this question is negative.

The image processing results of the “TLE + NLM” order and the “NLM + TLE” order are shown in Figure 10. As demonstrated, there is little difference in the visual effect between the processing results of the two cases. Upon observing the grayscale profiles, it can be found that the grayscale fluctuations of the enhanced images corresponding to the “TLE + NLM” case are slightly larger than those of “NLM + TLE”. The main reason for this is that the TLE algorithm has a stronger amplification effect on non-smoothed grayscale fluctuations, and texture enhancement before image denoising makes the TLE algorithm’s amplification effect more significant to some extent. However, applying the TLE algorithm before denoising may negatively impact image quality. Since the TLE algorithm will enhance texture details and speckle noise indiscriminately, applying the TLE algorithm before denoising will cause speckle noise to be amplified to a greater extent, which will increase the difficulty of subsequent noise suppression and easily lead to more residual speckle noise. As shown in Figure 10, some grayscale changes caused by speckle noise rather than internal wave stripes in the original images have disappeared in the grayscale profiles of the “NLM + TLE” case, while they still exist in the grayscale profiles of the “TLE + NLM” one. This indicates that applying the TLE algorithm first negatively affects the effectiveness of the subsequent denoising step, increasing the residual speckle noise.

Similar conclusions can be drawn from Table 5. As shown, there is not much difference in texture indexes between the two orders, but the *ENL* of the “TLE + NLM” order is significantly smaller than that of “NLM + TLE”. It suggests that applying the TLE algorithm before the NLM filtering limits the denoising effect of the NLM filtering. It should be noted that among the objective indexes of Data3, the *ENL* of the “TLE + NLM” order is smaller than that of the original image. This indicates that in some extreme cases, applying the TLE algorithm before the NLM filtering may even prohibit the NLM filtering from achieving the desired effect, resulting in a decrease in image quality. In conclusion, compared with the “NLM + TLE” order, the “TLE + NLM” order may not be an effective solution.

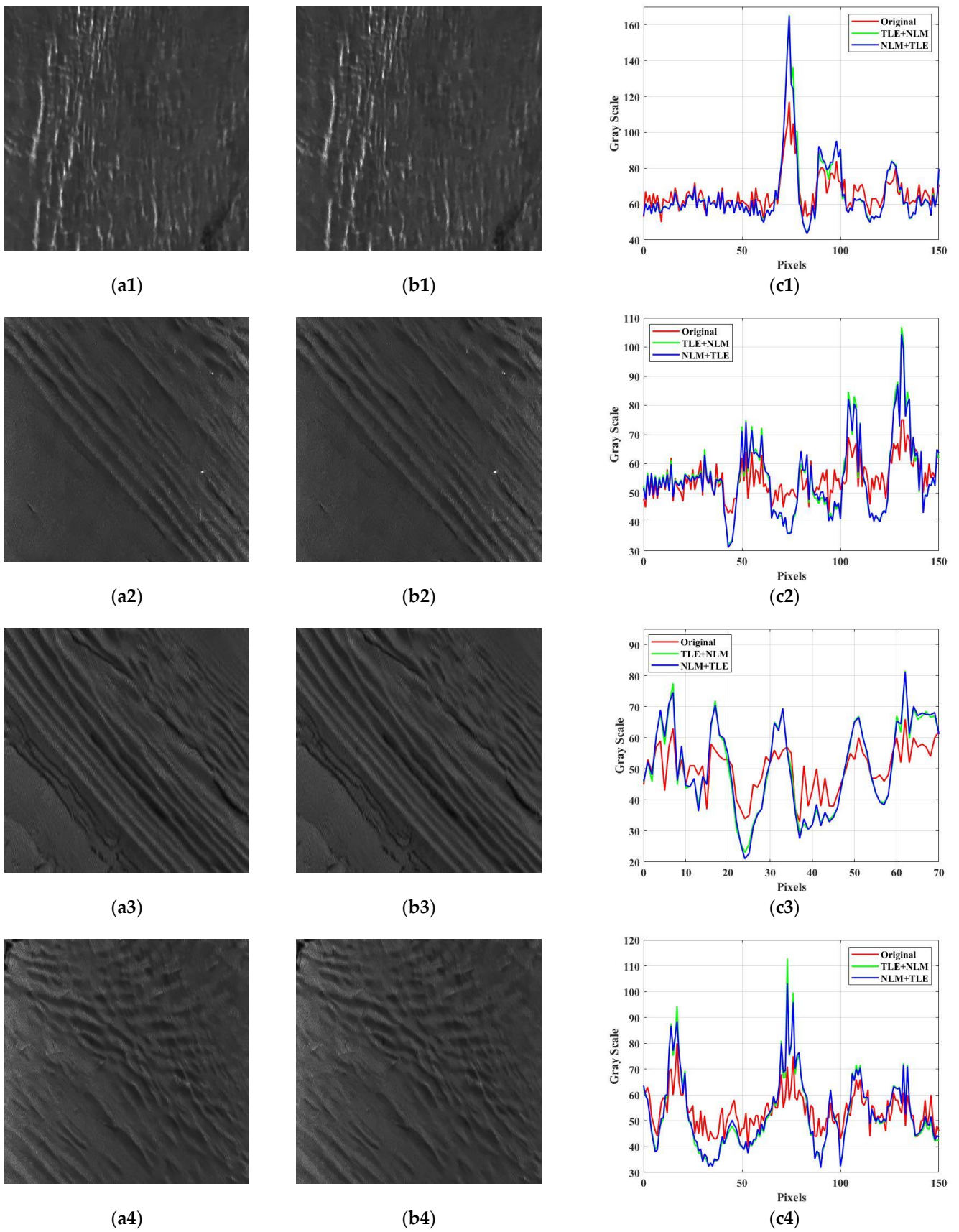
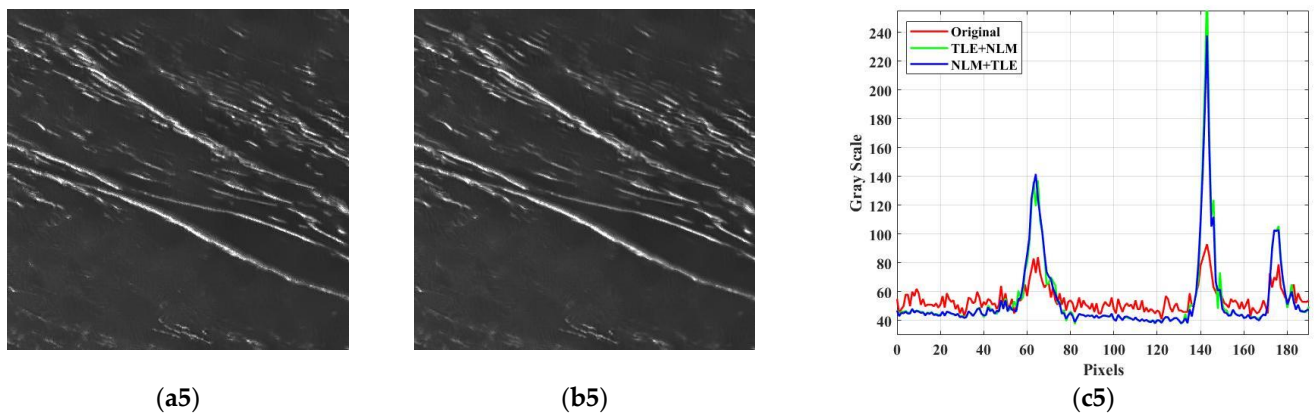


Figure 10. Cont.



**Figure 10.** Image processing results of the “TLE + NLM” order and the “NLM + TLE” order: (a1–a5) are the processing results of Data1–Data5 with the “TLE + NLM” order, respectively; (b1–b5) are the processing results of Data1–Data5 with the “NLM + TLE” order, respectively; (c1–c5) are grayscale profiles of the processing results of Data1–Data5 with the two orders, respectively, and the positions of grayscale profiles are the same as in Figure 7.

**Table 5.** Objective indexes of processing results of the two orders.

		<i>ENL</i>	<i>m</i>	<i>Var</i>	<i>C</i>	<i>S<sub>BD</sub></i> (dB)	$\Delta\sigma_w^0$ (dB)
Data1	Original	35.67	58.45	109.92	0.35	1.00	0.54
	TLE + NLM	57.66	57.94	581.01	1.02	1.83	1.96
	NLM + TLE	58.95	57.94	583.83	1.02	1.83	2.00
Data2	Original	41.60	54.37	36.25	0.23	0.79	0.14
	TLE + NLM	93.38	54.29	182.45	0.55	1.75	0.59
	NLM + TLE	95.54	53.79	172.87	0.52	1.76	0.60
Data3	Original	29.11	60.03	58.12	0.30	1.10	0.24
	TLE + NLM	25.55	64.49	191.09	0.56	2.13	0.74
	NLM + TLE	35.88	64.01	190.74	0.54	2.17	0.78
Data4	Original	42.21	60.65	44.51	0.25	0.89	0.18
	TLE + NLM	62.77	63.16	156.43	0.48	1.76	0.59
	NLM + TLE	79.81	62.72	154.90	0.46	1.77	0.62
Data5	Original	31.82	55.47	99.97	0.37	1.09	0.38
	TLE + NLM	147.76	55.01	1019.43	1.38	2.56	2.31
	NLM + TLE	162.29	54.83	967.30	1.30	2.53	2.31

## 5. Conclusions

A texture enhancement method for oceanic internal wave SAR images based on a combination of NLM filtering and the TLE algorithm has been proposed in this paper. In order to achieve internal wave texture enhancement, the internal wave image is first decomposed into the structure layer and the texture layer; then, a texture layer enhancement method targeting the texture characteristics of oceanic internal wave SAR images is applied; finally, the structure layer and the enhanced texture layer are combined to reconstruct the final enhanced image. The experimental results demonstrate that the TLE algorithm proposed in this paper can significantly enhance the texture details of oceanic internal wave SAR images, but it also increases the intensity of speckle noise, which hinders the improvement of image quality. To avoid the interference of speckle noise on texture enhancement, it was proposed to perform NLM filtering first to suppress speckle noise before applying the TLE algorithm for texture enhancement. As shown by the experimental results, NLM filtering can achieve a satisfactory balance between denoising and preserving texture features, which lays a sound foundation for the subsequent texture enhancement step. After verifying the effectiveness of both NLM filtering and the TLE algorithm, a

comparison between the proposed method and the method in [10] was carried out, and it was shown that the proposed method has a more superior performance in suppressing speckle noise, maintaining the overall image brightness, and enhancing internal wave texture details, all of which lead to significantly improved image quality.

Furthermore, the effect of the order of NLM filtering and the TLE algorithm on the improvement of internal wave image quality was also studied, and it has been shown that performing NLM filtering first and then the TLE algorithm can suppress speckle noise to a greater extent while ensuring significant texture enhancement, making it a more desirable processing order.

Although the NLM filtering performs well in both denoising and texture detail preservation, its processing time is significantly affected by the size of SAR images. Therefore, the efficiency of NLM filtering for processing large-scene oceanic internal wave SAR images needs to be improved. In the future, we will conduct additional research on enhancing the efficiency of denoising internal wave images, and attempt to adopt other denoising methods, such as deep learning-based methods, to improve the overall efficiency of the internal wave image texture enhancement process.

**Author Contributions:** Z.C., Y.G. and H.Z. implemented the methods and conceived and designed the experiments; Z.C. and Y.W. performed the experiments and analyzed the data; H.Z., W.Y. and W.L. supervised the research; Z.C. wrote the paper. All authors have read and agreed to the published version of the manuscript.

**Funding:** This research was funded by the National Key Research and Development Program of China, grant number 2023YFC3305901.

**Data Availability Statement:** Data are contained within the article.

**Conflicts of Interest:** The authors declare no conflicts of interest.

## References

1. Chong, J.; Ouyang, Y.; Li, F.; Zhu, M. *Synthetic Aperture Radar Image for Oceanic Internal Wave Detection*; China Ocean Press: Beijing, China, 2010; pp. 1–5.
2. Wang, T.; Huang, X.; Zhao, W.; Zheng, S.; Yang, Y.; Tian, J. Internal Solitary Wave Activities near the Indonesian Submarine Wreck Site Inferred from Satellite Images. *J. Mar. Sci. Eng.* **2022**, *10*, 197. [[CrossRef](#)]
3. An, J. Research on Near Field High Resolution SAR Image Enhancement Method. Master's Thesis, University of Electronic Science and Technology of China, Chengdu, China, 2017.
4. Wang, H.; Zhang, Y.; Shen, H.; Zhang, J. Review of Image Enhancement Algorithms. *Chin. Opt.* **2017**, *10*, 438–448. [[CrossRef](#)]
5. Tu, K. Research on Improvement of High Resolution SAR Image Quality. Master's Thesis, National University of Defense Technology, Changsha, China, 2013.
6. Cho, D.W.; Bui, T.D. Fast Image Enhancement in Compressed Wavelet Domain. *Signal Proc.* **2014**, *98*, 295–307. [[CrossRef](#)]
7. Carlson, G.E. Wavelet Processing of SAR Ocean Wave Images. In Proceedings of the Geoscience Remote Sensing Symposium, Firenze, Italy, 10–14 July 1995.
8. Fan, S.; Kudryavtsev, V.; Zhang, B.; Perrie, W.; Chapron, B.; Mouche, A. On C-Band Quad-Polarized Synthetic Aperture Radar Properties of Ocean Surface Currents. *Remote Sens.* **2019**, *11*, 2321. [[CrossRef](#)]
9. Bai, H.; Wang, X.; Chen, Y. A New Curvelet-Based Method for SAR Image Feature Enhancement. *J. Univ. Chin. Acad. Sci.* **2011**, *28*, 228–234.
10. Chen, Z.; Zeng, H.; Yang, W.; Chen, J. Texture Enhancement Method of Oceanic Internal Waves in SAR Images Based on Non-Local Mean Filtering and Multi-Scale Retinex. In Proceedings of the 2022 3rd China International SAR Symposium (CISS), Shanghai, China, 2–4 November 2022.
11. Alpers, W.R. Theory of Radar Imaging of Internal Waves. *Nature* **1985**, *314*, 245–247. [[CrossRef](#)]
12. Thompson, D.R.; Gasparovic, R.F. Intensity Modulation in SAR Images of Internal Waves. *Nature* **1986**, *320*, 345–348. [[CrossRef](#)]
13. Ouchi, K. On the SAR Imaging Mechanisms of Oceanic Internal Waves. In Proceedings of the IGARSS'93-IEEE International Geoscience and Remote Sensing Symposium, Tokyo, Japan, 18–21 August 1993.
14. Alpers, W.; Huang, W. On the Discrimination of Radar Signatures of Atmospheric Gravity Waves and Oceanic Internal Waves on Synthetic Aperture Radar Images of the Sea Surface. *IEEE Trans. Geosci. Remote Sens.* **2011**, *49*, 1114–1126. [[CrossRef](#)]
15. Fan, K.; Chen, P.; Gu, Y.; Li, X.; Meng, L.; Zhou, W. *Marine Remote Sensing and Image Interpretation of Spaceborne Synthetic Aperture Radar*; China Ocean Press: Beijing, China, 2017; pp. 25–26.
16. Lund, B.; Graber, H.C.; Xue, J.; Romeiser, R. Analysis of Internal Wave Signatures in Marine Radar Data. *IEEE Trans. Geosci. Remote Sens.* **2013**, *51*, 4840–4852. [[CrossRef](#)]

17. Buades, A.; Coll, B.; Morel, J.M. A Non-Local Algorithm for Image Denoising. In Proceedings of the 2005 IEEE Computer Society Conference on Computer Vision and Pattern Recognition (CVPR'05), San Diego, CA, USA, 20–26 June 2005.
18. Xu, L.; Yan, Q.; Xia, Y.; Jia, J. Structure Extraction from Texture via Relative Total Variation. *ACM Trans. Graph.* **2012**, *31*, 139. [[CrossRef](#)]
19. Cai, Y.; Chong, J. Parameter Assessment for Texture Feature Quality Evaluation in SAR Ocean Image. In Proceedings of the 2009 2nd Asian-Pacific Conference on Synthetic Aperture Radar, Xian, China, 26–30 October 2009.
20. Lee, J.S. A Simple Speckle Smoothing Algorithm for Synthetic Aperture Radar Images. *IEEE Trans. Syst. Man Cybern.* **1983**, *13*, 85–89. [[CrossRef](#)]
21. Parrilli, S.; Poderico, M.; Angelino, C.V.; Verdoliva, L. A Nonlocal SAR Image Denoising Algorithm Based on LLMMSE Wavelet Shrinkage. *IEEE Trans. Geosci. Remote Sens.* **2012**, *50*, 606–616. [[CrossRef](#)]
22. Dabov, K.; Foi, A.; Katkovnik, V.; Egiazarian, K. Image Denoising by Sparse 3-D Transform-Domain Collaborative Filtering. *IEEE Trans. Image Process.* **2007**, *16*, 2080–2095. [[CrossRef](#)] [[PubMed](#)]

**Disclaimer/Publisher’s Note:** The statements, opinions and data contained in all publications are solely those of the individual author(s) and contributor(s) and not of MDPI and/or the editor(s). MDPI and/or the editor(s) disclaim responsibility for any injury to people or property resulting from any ideas, methods, instructions or products referred to in the content.